Small angle neutron and X-ray studies of carbon structures with metal atoms

V T Lebedev[1], A A Szhogina[1], V Yu Bairamukov[1]

[1] Petersburg Nuclear Physics Institute, NRC Kurchatov Institute, 188300 Gatchina, Leningrad distr., Russia

vlebedev@pnpi.spb.ru

Abstract. Encapsulation of metal atoms inside carbon single-wall cages or within multi-layer cells has been realized using molecular precursors and high temperature processes transforming them into desirable structures. Endohedral fullerenols Fe@$C_{60}(OH)_X$ with 3d-metal (iron) have been studied by SANS in aqueous solutions where they form stable globular clusters with radii R_C ~ 10-12 nm and aggregation numbers N_C ~ 10^4. This self-assembly is a crucial feature of paramagnetic fullerenols as perspective contrast agents for Magneto-Resonance Imaging in medicine. Cellular carbon-metal structures have been created by the pyrolysis of diphthalocyanines of lanthanides and actinides. It was established that these ultra porous matrices consist of globular cells of molecular precursor size (~ 1 nm) which are aggregated into superstructures. This provides retain of metal atoms inside matrices which may serve for safety storage of spent fuel of nuclear power plants.

1. Introduction

Carbon structures have a great potential for various applications in biomedicine, electronics, alternative energy sources, ecology etc. that stimulates a progress in their synthesis and chemical modification [1-5]. Among them it should be mentioned a variety of endometallofullerenes (EMF), M@C_{2n} ($2n$ = 60; 70; 76; 80; 82 …), with rare earth elements (M) and especially new structures encapsulating paramagnetic 3d-elements [6-10]. Presently the EMFs are considered as advanced agents for Magneto-Resonance Imaging in medical diagnostics to improve its efficiency and spatial resolution without overdosing and side effects [11]. On the other hand, fullerenes and EMFs promise a progress in therapy for various diseases including neurodegenerative pathologies also since their water-soluble forms are able to overcome blood-brain barrier [12,13]. However, there is a substantial limitation for biomedical applications of carbon structures. It concerns a preparation of very pure fullerenes C_{60} and C_{70}. Recently basic principles and the ways of preparation of high quality fullerenes C_{60} and C_{70} there were developed [14,15]. Along with it, these authors pursued the aim to obtain new EMFs with 3d-metals. Finally, it was synthesized a new complex Fe@C_{60} with paramagnetic atom [16]. For a long time a creation of such molecules was not successful until a special precursor (iron phthalocyanine) has been found. Further it was embedded into carbon electrodes used for electric arc generating plasma of ionized carbon and metal which create desirable new compound of Fe@C_{60}. In hydroxylation process it was transformed into water-soluble form of Fe@$C_{60}(OH)_X$ (X ~ 30) [16].

Advances in synthesis of water-soluble forms of fullerenes and EMFs make possible their integration into biomedicine. For this purpose it is necessary a fundamental knowledge of structural

features and behaviours of these objects in aqueous solutions by means of neutron and X-ray scattering [17-19].

Water-soluble fullerenes and EMFs exhibit different kinds of assembly into fractal structures (linear or branched molecular chains, globular clusters). The features of such supramolecular organization at scales of 10^0 -10^2 nm depend on molecular concentrations and pH-factor in solutions [10, 17-21]. Suspected mechanisms of carbon structures ordering in solutions involve the contributions of hydrogen bonds, van-der-Waals' and hydrophobic interactions as well as dipole electric and magnetic forces if paramagnetic atoms are confined in carbon cages. Since the behavior of $Fe@C_{60}(OH)_X$ fullerenols governed by various interactions is not predictable, this became a subject of present study.

There was carried out the X-ray analysis of atomic structure of $Fe@C_{60}(OH)_X$ powders [16]. Further by SANS we have studied self-assembly peculiarities for fullerenols in aqueous media. In a series of measurements we increased the concentration towards the threshold of solubility and then decreased to get initial solution. This enabled us to check a reversibility of fullerenols' assembly.

The second part of experiments is devoted to the structural analysis of carbon matrices built of tiny cells with metal atoms captured during pyrolysis of diphthalocyanines (DPC). In these molecules metal atoms (Y, La, Ce, Nd, Tb, U) are coordinated between plane ligands [22]. In neutral atmosphere at high temperatures (800-1700 ^oC) the molecules in DPC-powders due to destruction have lost light elements (H, N, O). Such samples are ultra porous matrices where metal atoms are localized inside carbon cells which are aggregated. The X-ray study was aimed to determine cells' structural features (dimensions, atoms aggregation numbers) inside matrices at various conditions of pyrolysis [23].

2. Experimental

2.1. Endofullerenes, synthesis and attestation

The synthesis of endofullerenes was carried out in electric-arc (current of 130 A, helium atmosphere, pressure of 380 mm Hg) by the evaporation of carbon electrodes filled with a mixture of graphite and iron phthalocyanine pyrolysate (iron content ~ 10% wt.). To remove residual iron not involved into endohedral complexes, fullerene-containing soot was etched in dilute hydrochloric acid. First, empty fullerenes (C_{60}, C_{70} and higher homologues) were extracted from the soot in o-xylene. Second, the EMFs were isolated from the soot by extraction in N,N-dimethylformamide containing reducing agent to enhance the process efficiency.

After solvent evaporation and drying, solid EMF-extract was examined by X-ray fluorescence analysis (XRF) which showed iron amount (2.4 – 4.8 % wt.). Further this product was hydroxylated in dilute aqueous solution of hydrogen peroxide (65° C) and mixed with a tenfold volume of precipitating mixture (isopropyl alcohol and hexane, ratio 9:1). Finally the precipitate separated by centrifugation was dried under vacuum (80°C, 3 hours). The concentration of iron in resulting product was of 3% wt. (XRF data).

The amount of hydroxyl groups attached to a fullerene cage, $X = 30 \pm 2$, was found by thermo-gravimetric analysis (TGA)[24]. The prepared sample contained 70 % of $Fe@C_{60}(OH)_{30}$ and empty fullerenols $C_{60}(OH)_{30}$ in the remainder and had a solubility of 46 mg/ml.

The molecular structure of the powders of $C_{60}(OH)_{30}$ (reference sample) and $Fe@C_{60}(OH)_{30}$ has been studied by X-Ray diffraction [16]. Chemical bonding hydroxyl groups was confirmed by Fourier Transform Infrared Spectroscopy (FTIR). The FTIR-spectrum of carbon-metal structure showed characteristic frequencies for chemical bonds in molecules of $Fe@C_{60}(OH)_{30}$ (figure 1), i.e. broad band at 3412 cm^{-1} for stretching mode of OH groups and other peaks at 1620 cm^{-1} (C=C), 1390 cm^{-1} (C-OH) and 1150 cm^{-1} (C-OH).

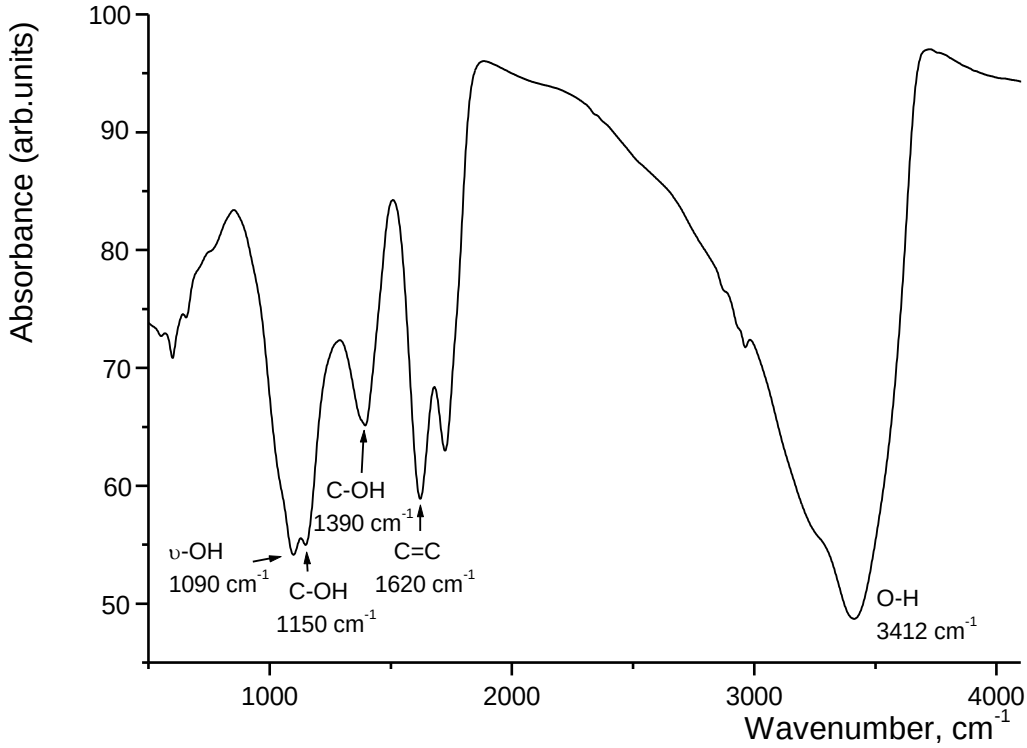

Figure 1. FTIR absorption spectrum for $Fe@C_{60}(OH)_{30}$.

Eventually the detailed analysis enabled us to identify the endohedral structure of new carbon-iron compound [16]. In following SANS experiments fullerenols' ordering in aqueous media has been studied taking into account actual scientific and practical aspects for biomedical applications.

2.2. SANS on fullerenols in aqueous solutions

In light water $Fe@C_{60}(OH)_{30}$ molecule has a good contrast in neutron scattering. This provides the SANS-measurements even at low concentrations. Varying the concentrations (C = 0.24 – 3.9 % wt.), we started from dilute solutions and moved to the threshold of solubility (46 mg/ml). In a series of experiments we collected the SANS-data at ambient temperature in the range of momentum transfer $q = (4\pi/\lambda)\sin(\theta)$ = 0.04-0.8 nm^{-1} (scattering angles 2θ, neutron wavelength λ = 0.3 nm, $\Delta\lambda/\lambda$ = 0.25, "SANS-Membrane", PNPI). Next measurements we carried out using dilution from maximum to minimum concentration to test reversibility in fullerenols' ordering (figure 2).

In both series, the scattering intensities $I(q)$ demonstrate a huge grow (figure 2) at low momentum transfer, q < 0.4 nm^{-1}. This testifies a strong molecular clustering at the scales ~ $2\pi/q \geq 10^1$ nm. The data in the first series showed a similarity of SANS-profiles shifted in logarithmic scale with concentration rise. The experiments by a dilution exhibited qualitatively the same results. In the first approximation all the data obey the scattering law

$$I(q) = I_0\left[1 + (qR_C)^2\right]^{-2} . \quad (1)$$

The parameters I_o and R_C denote forward intensity and correlation radius of molecular clusters. Taking into account a proportionality of intensity parameter $I_o \sim CN_C$ to concentration and aggregation number (N_C), we used normalization $I_o/C \sim N_C$ to reveal the concentration dependence of fullerenols' aggregation degree (figure 3).

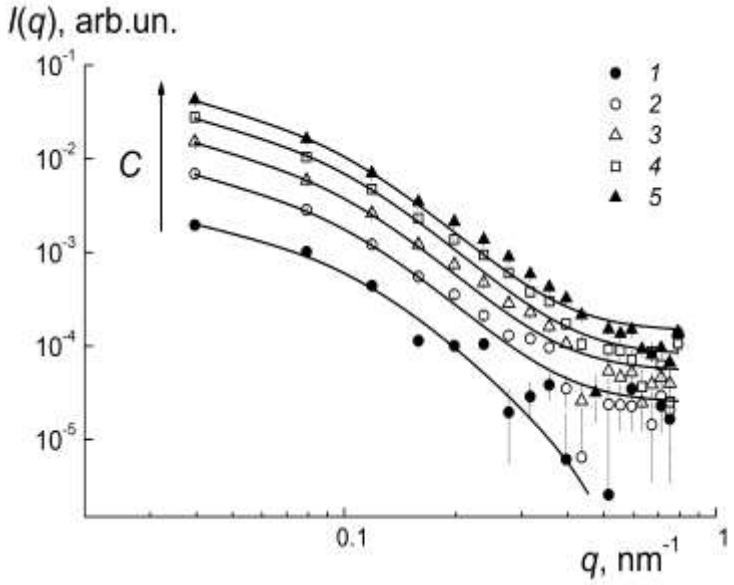

Figure 2. SANS from $Fe@C_{60}(OH)_X$ aqueous solutions (20°C) by the increase of concentration (*C*, wt.%):1 - 0.24; 2 – 0.67; 3 – 1.4; 4 – 2.5; 5 – 3.9. Lines are fitting functions (1).

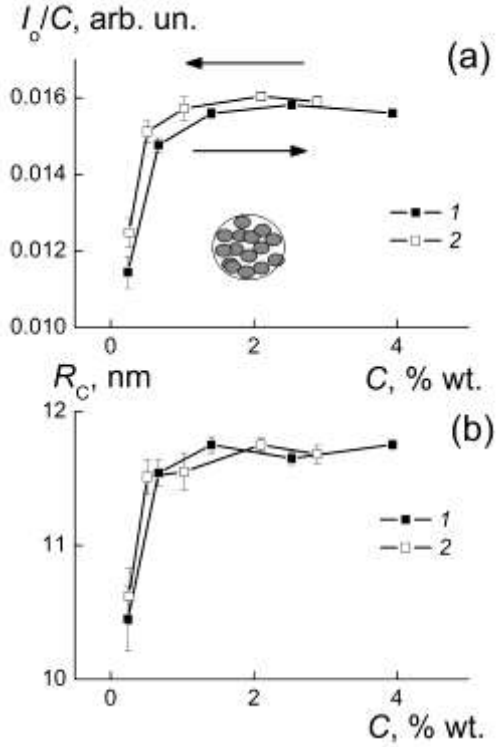

Figure 3. Concentration dependencies of scattering function (1) parameters in solutions with increasing (1) and decreasing (2) fullerenols' content: (a) - forward intensities normalized to concentrations, $I_o(C)/C$; (b) - correlation radii $R_C(C)$ vs. fullerenols' content.

The parameters I_o/C and R_C come upward when concentration increase and achieve saturation at $C \geq 1$ % wt. A reverse dilution of concentrated system does not provide a complete repeat of the parameter $I_o/C \sim N_C$ being a measure of aggregation. The aggregation numbers still remain greater (~ 3 %) by dilution comparatively to concentrating process. Hence, a weak hysteresis in aggregation numbers' behavior exists (figure 3). The N_C magnitudes were computed using the parameters I_o and taking into account the contrast of fullerenols in water and their volume fractions. These high aggregation numbers cover the range of $N_C = (1.1\text{-}1.6)10^4$. Meanwhile the correlation radii of clusters demonstrate a moderate growth, $R_C \sim$ 10-12 nm, without a hysteresis.

Summarizing the results it is worth to note that iron containing fullerenols in aqueous solutions are ordered into stable clusters. Their dimensions and aggregation degrees are not sensitive to strong

changes in molecular concentrations. Therefore, these stable small-sized structures with paramagnetic metal atoms seems to be attractive for biomedical applications with dosing variations in living organisms without substantial risks of irreversible sedimentation.

Another kind of carbon structures with metal has been created by the pyrolysis of molecular compounds that provides a formation of porous matrices which strongly hold heavy metals and nuclides [26].

2.3. Pyrolysates of diphthalocyanines of metals, synthesis and structure by X-Ray scattering

Pursuing the aim of reliable isolation of nuclides inside solid matrices, there were developed chemical methods to bond radioactive elements [27]. For preparation of carbon matrices to encapsulate metal atoms, the precursors on the base of diphthalocyanines of metals (M = Y, La, Ce, Nd, Tb, Sm, U) have been synthesized. The methods of their preparation, structure and properties are described in detail [27,28].

A molecule of diphtalocyanine Pc_2M is composed of two ligands (Pc) connected via a metal atom (Figure 4). Pyrolysis of diphtalocyanine (argon atmosphere; temperature 800–900°C) causes molecular destruction with a release of hydrogen, nitrogen and other gases. As a result, in a molecule the carbon atoms at the edges of ligands can be linked via free bonds into a cell similar to fullerene cage. In such a cell (size ~ 1 nm) even ten metal atoms can be easily placed. Upon pyrolysis of diphtalocyanine, monomolecular cells create ultra porous metal–carbon structure, MC_X (X ~ 30–35), with molecular-sized and larger intermolecular voids (~10^0–10^3 nm) [23]. The incorporation of nuclides into the voids of matrix can provide their safe storage. Because of small-sized size holes, a carbon matrix is penetratable only for atoms with radius less than 0.12–0.13 nm. The most of nuclides can leave carbon cells only under their destruction or strong deformation at the temperatures above 1400°C. Below 1000°C a confinement for almost all studied radioactive elements in matrices is close to 100% [27].

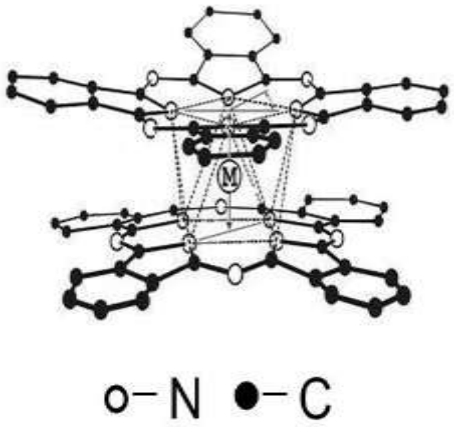

Figure 4. Structure of diphtalocyanine molecule with metal atom (M) between ligands. Nitrogen and carbon atoms are shown.

In X-ray experiments we have studied the structures of carbon cells in pyrolysates with various elements (Y, La, Ce, Nd, Tb, Sm, U) synthesized at 800–1700°C [27]. The powders of pyrolysates were examined at ambient temperature (Diffractometer "Dron-3M", CuK_α radiation, wavelength λ = 0.154 nm) in the interval of scattering vector modules $q = (4\pi/\lambda)\sin(\theta)$ = 7-80 nm^{-1} at the degrees 2θ = 10-150°.

Characteristic data for La-pyrolysates (figure 5) illustrate scattering patterns for the specimens completely amorphous (low-temperature synthesis, T < 1000 °C) and for high temperature materials (T > 1000 °C) containing La-carbide precipitates and crystalline graphite domains coexisting with amorphous phase [28]. The scattering intensities $I(q)$ for low-temperature pyrolysates (800-900 °C) demonstrate broad peaks at q_1 ~ 15-20 nm^{-1}, q_2 ~ 25-40 nm^{-1} and q_3 ~ 45-60 nm^{-1}. In the case of high-temperature pyrolysis (1020 °C), peaks' positions are defined more exactly, $q_{1m} \approx 19$ nm^{-1}, $q_{2m} \approx 30$ nm^{-}

[1], $q_{3m} \approx 50$ nm^{-1}. This enables us to estimate the periods $L_1 = 2\pi/q_{1m} \approx 0.33$ nm, $L_2 \approx 0.21$ nm and $L_3 \approx 0.13$ nm.

The smallest parameter L_3 corresponds to the length of carbon-carbon bond, while the others should be attributed to the distances between atomic planes. The L_2 is close to the period of graphite hexagonal lattice $a = 0.246$ nm, and the $L_1 \approx d_{002} = c/2 = 0.335$ nm is a half of c-period [29]. Thus, the data for high temperatures ($T > 1000$ ºC) testify atomic order in pyrolysates like in crystalline graphite (figure 5).

In this study we tried to detect subtle structural features of amorphous phase which is not amenable to ordinary X-ray diffraction analysis. Therefore we subtracted the contributions $I_C(q)$ of narrow peaks related to crystal order and approximated by Gaussians. The data were corrected also for background, $I_S(q) = I(q) - I_C(q) - Bg$. Further we used final data to evaluate short range correlations of atoms in these ultra porous structures.

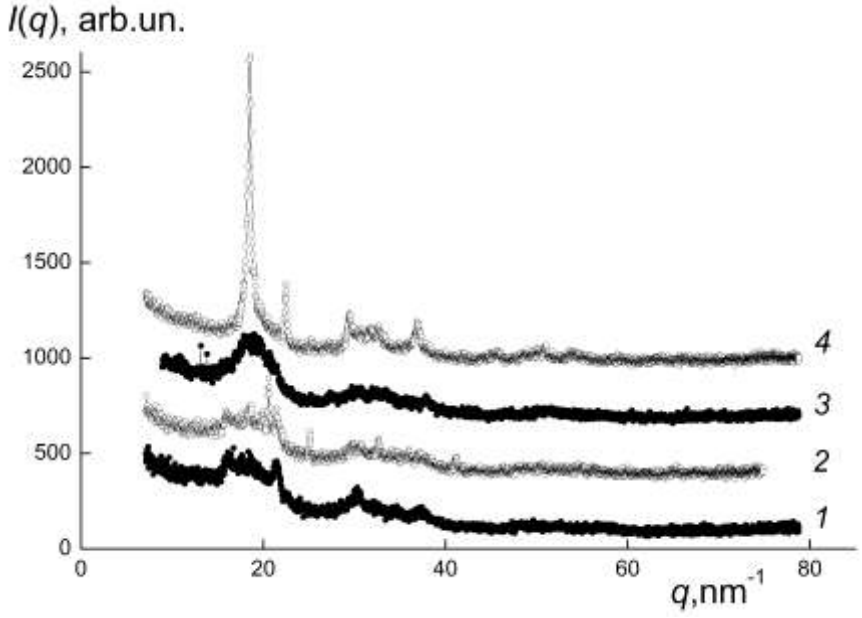

Figure 5. Diffraction patterns for La-pyrolysates synthesized at 800; 900; 1020; 1600 ºC (1-4). Curves are shifted for clear presentation.

2.4. Atomic correlations in pyrolysates

For pyrolysates the spectra of atomic correlations [25] are given by Fourier-transform of scattering intensities $I_S(q)$,

$$\gamma(R) \sim < \Delta\rho_e(0) \cdot \Delta\rho_e(R) > \sim \left[\frac{1}{2\pi}\right]^3 \int I_S(q) [\frac{\sin(qR)}{(qR)}] 4\pi q^2 dq \quad . \qquad (2)$$

As usual, the $\gamma(R)$ is defined by local deviations of electron density, $\Delta\rho_e(0)$ and $\Delta\rho_e(R)$, from a middle level in the sample when two points are separated by a certain distance R and there is averaging over all possible positions of pairs in sample's volume. For our isotropic samples the spectra are presented in the form $G(R) = R^2\gamma(R)$ which shows spatial correlations between a scattering center and surrounding centers at spherical surface (radius R) (figure 6).

For low-temperature structures (figure 6a) it is visible that the edge of the intense peak quite exactly corresponds to the distance d_{002} between graphene planes in graphite crystal. Indeed, if the atoms belong to neighboring planes with spacing d_{002}, their cross-correlations start at $R \geq d_{002}$. In frames of a simple model [30] for uniform thin parallel planes (discrete positions of atoms neglected) the $G(R)$ increases up to the maximum at $R_{max} = (4/3)^{1/2} d_{002} \approx 0.39$ nm. Really, the position of maxima ($R_{max} \sim$

0.4 nm) in spectra for low-temperatures pyrolysates are in agreement with this model. Meanwhile, only a rough accordance with characteristic periods in graphite crystal (d_{100}, $2d_{002}$) is observed since the peaks are shifted to lower radii (figure 6a). This can be interpreted as a result of curvature of plane fragments. Such fragments are formed of diphthalocyanine ligands (figure 4) which lost light atoms (H, N) by destruction. After partial destruction a molecule of diphthalocyanine probably is a structure like a carbon cage when ligands' edges are linked via free bonds. It means a transformation of plane ligands into curved structures which can be combined in multi-layer stacks. The high-temperature treatment stimulates a growth of compact (globular) structures when single-layer fragments become cross linked. As a result, in spectra neighboring partial peaks overlap and form a broad common hump (figure 6b). Its center position $R \sim 0.6$ nm indicates a characteristic radius of globules which are comparable in size to precursor molecules.

Along with it, the spectra are still modulated that indicates a multilayered structure of globules (figure 6b). In order to find the amount of atoms m (aggregation number) in globular entities we have taken into account the scattering lengths of atoms. Such a length is proportional to atomic number of element (Z). However, in dense matrix a length for each atom should be corrected for scattering length density of matrix. Thus, we used effective lengths (Z_{EC}, Z_{ELa}) for carbon and lanthanum to estimate atomic incoherent scattering intensities for the samples,

$$I_{01} = 4\pi S_1 \sim [\nu Z_{ELa}{}^2 + (1-\nu) Z_{EC}{}^2] \cdot$$

Here parameter S_1 is the integral area under the first peak in $G(R)$-spectrum. The integral represents the contributions of lanthanum and carbon atoms with atomic share ν and $(1-\nu)$ to the incoherent scattering cross section. Such a peak (maximum at $R \sim 0.1$ nm, figure 6) describes the scattering from electrons in single atoms.

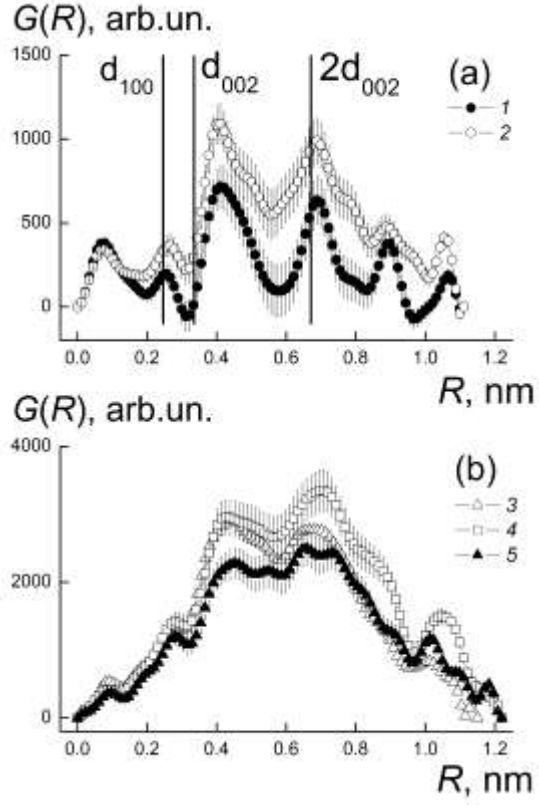

Figure 6. Spectra $G(R)$ for pyrolysates prepared at different temperatures: (a) 800 and 900 °C (1,2); (b) 1020; 1600 and 1800 °C (3,4,5). Straight lines denote the distances between atomic planes in graphite.

Meanwhile, it is overlapped with a peak arisen due to chemical bonds with neighboring atoms. The contribution of this incoherent scattering was found using approximation of $G(R)$-spectra by a sum of Gaussians in the limited range of radii ($0 \le R \le 0.3$ nm).

For each spectrum the incoherent intensity I_{o1} was compared to coherent one defined by the total area under the profile of *G(R)*-function,

$$I_0 \sim m[\nu Z_{ELa} + (1-\nu)Z_{EC}]^2 \quad .$$

Here the parameter *m* is a total atomic aggregation number for the structures observed in the experimental range of radii $R \leq 1$ nm. For matrices prepared at different temperatures we estimated this parameter from the ratio

$$m = \left[\frac{I_0}{I_{01}}\right] \cdot \frac{[\nu Z_{ELa}{}^2 + (1-\nu)Z_{EC}{}^2]}{[\nu Z_{ELa} + (1-\nu)Z_{EC}]^2}$$

.

Additionally, the integrals over *G*(*R*)-spectra give the gyration radii of aggregates (R_g) by formula [25]

$$R_g{}^2 = \frac{\frac{1}{2}\int G(R)R^2 dR}{\int G(R)dR}$$

The gyration radii and aggregations numbers for La-carbon structures are presented in figure 7 as dependent on synthesis temperature. The rise of pyrolysis temperature above 1000 °C induces a huge growth in aggregation degree, $m(T) \sim 100$. At the same time, the gyration radii of structures demonstrate only a weak increase, $R_g \sim 0.4$-0.5 nm. It means a formation of dense globules at high temperatures. Indeed, comparison of their masses ~ *m* and volumes ~ $R_g{}^3$ has shown that the density of high-temperature globules approaches to this parameter for graphite but yet remains lower by 16 %.

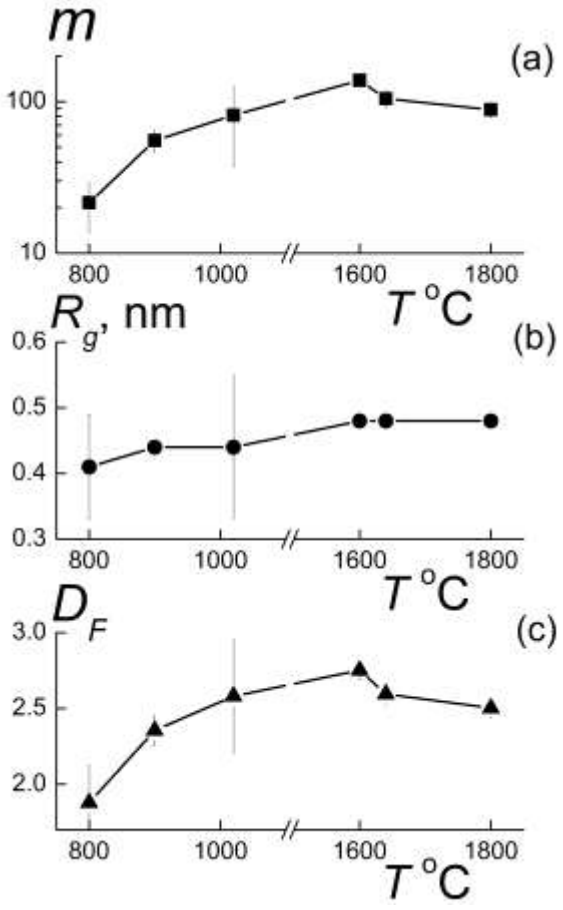

Figure 7. Structural parameters for La-pyrolysates vs. the temperature of treatment: (a) – aggregation number *m*(*T*); (b) – gyration radius $R_g(T)$; (c) – fractal dimension $D_F(T)$.

In general, these structures can be considered as fractal clusters with dimension

$$D_F(T) = \frac{\ln(m)}{\ln\left[\frac{R_g}{r_a}\right]}$$

where $r_A \approx 0.08$ nm is carbon atom radius. The obtained parameter $D_F(T) \sim 1.9\text{-}2.8$ strives upward in the temperature range 800-1600°C although in the upper limit (1800°C) it shows a downturn due to increased destruction (figure 7 c). Such structures may be formed via diffusion limited aggregation which leads to a growth of mass fractals when it is possible a transition from plane structures, $D_F \sim 2$, to branched 3D-aggregates, $D_F \sim 2.5\text{-}2.8 > 2$. These X-Ray studies have revealed small-sized (~ 1 nm) structures which serve as the building blocks. Their association creates multi-level aggregates (10^0-10^2 nm) forming solid matrices. The structural features of various matrices have been analyzed in neutron scattering experiments [23].

3. Conclusions

SANS-studies of new fullerenols $Fe@C_{60}(OH)_X$ have shown that these paramagnetic endohedral objects create stable self-assembled globular structures with moderate and reversible changes of parameters in aqueous solutions in a wide range of concentrations that is crucial for biomedical applications.

Carbon-metal materials prepared of diphthalocyanines and studied by X-ray scattering are characterized as ultra porous matrices composed of molecular-sized structures. By the increase of pyrolysis temperature (800-1800 °C) they undergo a transformation when molecular skeletons lose light atoms and again begin to integrate carbons to form multi-layer globules with high aggregation numbers ~ 100 but their gyration radii ~ 0.5 nm do not exceed the dimensions of diphthalocyanine molecule.

Thus, a combination of X-Ray and neutron scattering together with data treatment complementary in reciprocal and real space has provided a comprehensive analysis of the mechanisms of formation of different kinds of carbon-metal primary structures and understanding subtle features of their assembly into secondary clusters.

Acknowledgements

The work was supported by Russian Foundation for Basic Research (grant N 14-23-01015 ofi-m).

References

[1] *Nanomaterials for application in medicine and biology.* 2008 Ed M Giersig ang G B Khomutov. *Proc. of the NATO Advanced Research Workshop on Nanomaterials for Application in Medicine and Biology*, Bohn, Germany, 4-6 October 2006. (Springer, P.O.Box 17, 3300 AA Dordrecht, The Netherlands. p186)
[2] Avouris P, Chen Z, Perebeinos V 2007 *Nature Nanotechnology* **2** 605
[3] Nicholas R J, Mainwood A, Eaves L 2008 *Phil. Trans. R. Soc. A* **366** 189
[4] Nelson J 2011 *Materials Today* 14. N 10. P. 462-470.
[5] *Carbon nanomaterials sourcebook. Vol. 1. Graphene, Fullerenes, Nanotubes and Nanodiamonds*. 2016 Ed K D Sattler (University of Hawaii at Manoa, Honoluly, USA. CRC Press. Taylor&Francis Group, London, New York. p 591)
[6] Heath J R, O'Brien S C, Zhang Q, Liu Y, Curl R F, Tittel F K, Smalley R E 1985 *J. Am. Chem. Soc.* **107** 7779
[7] Shinohara H 2000 *Reports on Progress in Physics* **63** 843
[8] Koltover V K 2007 *Endohedral fullerenes: from chemical physics to nanotechnology and nanomedicine. In:* "*Progress in Fullerene Research*" (ed M Lang, New York: Nova Science Publishers, pp. 199-233)
[9] Kozlov V S, Suyasova M V, Lebedev V T 2014 *Russian Journal of Applied Chemistry* **87** 121

[10] Szhogina A A, Kulvelis Yu V, Lebedev V T, Sedov V P 2015 *Russian Journal of Applied Chemistry* **88** 2009
[11] Shevtsov M A, Nikolaev B P, Yakovleva L Y, Dobrodumov A V, Torok Gy, Lebedev V T, Pitkin E 2014 *Appl. Magn. Res.* **45** 339
[12] Harutyunyan A R, Pradhan B K, Sumanasekera G U, Korobko E Yu, Kuznetsov A A 2002
[13] *European Cells and Materials* **3** (Suppl. 2) 84
[14] Grushko Yu S, Sedov V P, Kolesnik S G 2012 *Method of producing fullerene C_{60}*
[15] (RF Patent N 2456233, Publ. 20.07.2012, Bull. №20, priority of the invention of 13.08.2010)
[16] Sedov V P, Szhogina A A, Lebedev V T, Chernenkov Yu P, Aksenov V L , Kovalchuk M V 2014 New endometallofullerenes incapsulating iron atoms. *Reprint of PNPI* N 2963, Gatchina p11
[17] Kyzyma E A, Tomchuk A A, Bulavin LA, Petrenko V I, Almasy L, Korobov M V, Volkov D S, Mikheev I V, Koshlan I V, Bláha P, Avdeev M V, Aksenov V L 2015 *Surface Investigation X-Ray, Synchrotron and Neutron Techniques* (Gordon and Breach Science Publishers, Switzerland) **9** 1
[18] Nikolaev I V, Lebedev V T, Grushko Yu S, Sedov V P, Shilin V A, Török Gy, Melenevskaya E Yu 2012 *Fullerenes, Nanotubes, and Carbon Nanostructures* **20** 345
[19] Lebedev V T, Kulvelis Yu V, Runov V V, Sedov V P, Szhogina A A 2015 *Journal of Optoelectronics and Advanced Materials* **17** 1193
[20] Lebedev V T, Kulvelis Yu V, Runov V V, Sedov V P, Szhogina A A 2014 *Journal of Surface Investigation. X-ray, Synchrotron and Neutron Techniques* (Pleiades Publishing, Ltd.) **8** 1044
[21] Suyasova M V, Kulvelis Yu V, Lebedev V T, Sedov V P 2015 *Russian Journal of Applied Chemistry* **88** 1839
[22] *The Phthalocyanines: properties and applications.* 1989 eds C C Leznoff, A B P Lever (New York: VCH Publ., p 436)
[23] Lebedev V M, Lebedev V T, Orlova D N, Sovestnov A E, Tikhonov V I 2014 *Journal of Surface Investigation. X-ray, Synchrotron and Neutron Techniques* (Pleiades Publishing, Ltd.) **8** 1002
[24] Goswami T, Kumar R., Alam S, Mathur G N 2004 *Thermochimica Acta* **419** 97
[25] Feigin L A, Svergun D I 1987 *Structure Analysis by Small-Angle X-Ray and Neutron Scattering* (Springer Science + Business Media New York) p 333
[26] Tikhonov V I, Moskalev P N, Kapustin V K 2008 *The carbon matrices made of pyrolised phthalocyanines as a base for encapsulation of the long-lived nuclides of iodine, technetium and minor actinides. Proc. 11th Int. Conf. on Environmental Remediation and Radioactive Waste Management ICEM-2007, Belgium. Report* №7084
[27] Tikhonov V I, Moskalev P N, Kapustin V K 2009 *Method of fixation of radionuclides for their stirage and transmutation* (RF Patent. N 2343575. Publ. 10.01.2009. Bull. N 1. Priority of the invention of 27.02.2007)
[28] Sovestnov A E, Kapustin V K, Tikhonov V I, Fomin E V, Chernenkov Yu P 2014 *Physics of the Solid State* **56** 1673
[29] Chung D D L 2002 *J. Material Sciences* **37** 1
[30] Lebedev V T, Sovestnov A E, Kapustin V K, Tikhonov V I, Chernenkov Yu P *Structure of Amorphous Phase of Pyrolysates of Lanthanun Diphyhalocyanines by X-Ray scattering* 2016 *Surface Investigation X-Ray, Synchrotron and Neutron Techniques, Gordon and Breach Science Publishers (Switzerland)* in press.